UC Irvine
UC Irvine Previously Published Works

Title
XACT-guided interventional procedures: A feasibility study

Permalink
https://escholarship.org/uc/item/8k96c9f3

Journal
Medical Physics, 53(4)

ISSN
0094-2405

Authors
Yan, Yuchen
Pandey, Prabodh Kumar
Xu, Yifei
et al.

Publication Date
2026-04-01

DOI
10.1002/mp.70401

Copyright Information
This work is made available under the terms of a Creative Commons Attribution License, available at https://creativecommons.org/licenses/by/4.0/

Peer reviewed

eScholarship.org Powered by the California Digital Library
University of California

Check for updates

Received: 22 September 2025 | Revised: 16 February 2026 | Accepted: 2 March 2026

DOI: 10.1002/mp.70401

RESEARCH ARTICLE

MEDICAL PHYSICS

XACT-guided interventional procedures: A feasibility study

Yuchen Yan[1] | **Prabodh Kumar Pandey**[2] | **Yifei Xu**[1] | **Leshan Sun**[3] | **Nadine Abi-Jaoudeh**[2] | **Zhehui Wang**[5] | **Shawn (Liangzhong) Xiang**[1,2,4]

[1]Department of Biomedical Engineering, University of California, Irvine, California, USA

[2]Department of Radiological Sciences, University of California, Irvine, California, USA

[3]Department of Radiation Oncology, Mayo Clinic, Phoenix, Arizona, USA

[4]Beckman Laser Institute, University of California, Irvine, California, USA

[5]Los Alamos National Laboratory, Los Alamos, New Mexico, USA

Correspondence
Shawn (Liangzhong) Xiang, Department of Biomedical Engineering, University of California, Irvine, CA, USA 92617.
Email: liangzhx@hs.uci.edu

Funding information
UCI Chao Family Comprehensive Cancer Center, Grant/Award Number: P30CA062203; National Institutes of Health, Grant/Award Numbers: R37CA240806, U01CA288351, R50CA283816

Abstract

Background: X-ray Induced Acoustic Computed Tomography (XACT) is an emerging imaging technique that provides 3D volumetric images from a single projection by detecting X-ray-induced acoustic (XA) waves with ultrasound (US) transducers. Unlike MRI or CT, XACT enables real-time 3D imaging without long acquisition times, 2D limitations, or motion artifacts from mechanical rotation. Furthermore, when integrated with conventional pulse-echo US through time-sequenced operation, XACT provides complementary soft-tissue contrast, establishing it as a promising platform for dynamic interventional radiology (IR) guidance.

Purpose: This study aims to evaluate the feasibility of XACT as a novel imaging tool for IR, specifically for guiding needle placement and monitoring contrast agent dynamics.

Methods: We developed a 3D XACT imaging system equipped with a 256-element 2D matrix array and a portable X-ray tube to visualize needle insertion and contrast agent dynamics. To capture both needle position and soft tissue anatomy, we integrated a dual-modality system combining XACT with pulse-echo US using a 128-element linear US array. Experiments were conducted on both tissue-mimic phantoms and soft tissue samples. GPU-accelerated algorithm has been developed for 3D XACT image reconstruction.

Results: The results demonstrate the 3D capabilities of XACT imaging for interventional procedures, including monitoring of needle placement and tracking of contrast agent dynamics. The imaging speed reached up to 3∼4 s per frame, constrained by the repetition rate of the X-ray source and signal to noise ratio. The dual-modality approach provided clear visualization of the needle's position and the surrounding soft tissue structures, achieving imaging resolution around 2 mm.

Conclusions: This study demonstrates that XACT imaging is feasible to be used for IR. Its 3D imaging capability with faster imaging speed would be an alternative to cone beam CT and its capability to combine US imaging will provide richer information for soft tissue

1 | INTRODUCTION

Interventional radiology (IR) procedures depend heavily on imaging technologies for accurate needle placement and real-time monitoring of contrast agent delivery[1] While existing modalities provide critical guidance, each has inherent limitations[2–6] Magnetic resonance imaging (MRI) offers superb soft-tissue contrast, which is ideal for anatomical delineation[7] However, its long acquisition times, limited accessibility, and the need for specialized equipment restrict its utility in time-sensitive, dynamic procedures[8,9] X-ray fluoroscopy, widely used in IR, provides real-time imaging with high temporal resolution but is fundamentally limited to two dimensions, offering no depth information and making 3D navigation challenging[4,10] Cone-beam computed tomography (CBCT) provides high-resolution 3D imaging, but only through rotational acquisition over several seconds,

© 2026 American Association of Physicists in Medicine.

which introduces motion artifacts and renders it unsuitable for continuous, real-time imaging during dynamic interventions[11,12]

These limitations point to a need for an imaging platform that combines the strength of current technologies—real-time, 3D imaging, and with soft-tissue contrast[13,14] To address this gap, we have developed a novel imaging technique called X-ray Induced Acoustic Computed Tomography (XACT)[15–18] XACT leverages short-pulsed X-ray beams to generate acoustic waves in tissue, which are then detected by ultrasound (US) transducer to reconstruct volumetric images[15–17,19] Unlike CBCT, XACT can produce 3D images from a single X-ray projection[20] eliminating the need for mechanical rotation and reducing susceptibility to motion artifacts, thus making it a promising candidate for real-time guidance in 3D.

Previous studies have validated XACT's performance in static imaging scenarios, including breast imaging[21,22] bone mapping[23–26] and molecular contrast detection[27,28] Recently, XACT has demonstrated its capability of 3D imaging with a single projection. However, its capability for capturing dynamic processes—such as needle tracking or monitoring the flow of contrast agents-remained unproven. Moreover, while X-ray-based imaging techniques generally lack strong soft-tissue contrast[29,30] XACT can be combined with conventional pulse-echo US in a single platform offers soft-tissue visualization[15] This dual-modality approach has the potential to provide rich anatomical and functional information during interventional procedures, improving accuracy and safety.

In this study, we demonstrated the feasibility of the 3D capabilities of XACT imaging for interventional procedures, including monitoring of needle placement and tracking of contrast agent dynamics in 3D. We have also demonstrated a dual-modality system that integrates XACT with pulse-echo US, enabling clear visualization of the needle trajectory and surrounding soft-tissue structures. Together, these developments establish XACT as a promising platform for next-generation interventional imaging.

2 | MATERIALS AND METHODS

2.1 | Theory of XACT imaging

The evolution of X-ray induced acoustic waves is governed by[31,32]:

$$\frac{\partial^2 p\left(\vec{r},t\right)}{\partial t^2} - c^2\nabla^2 p\left(\vec{r},t\right) = \Gamma H\left(\vec{r}\right)\frac{\partial \delta\left(t\right)}{\partial t}, \tag{1}$$

with Γ being the Gruneisen parameter, c being the sound speed in the medium. H represents the X-ray energy deposition, and the initial pressure source. The solution to Equation (1) is given by[33]:

$$p\left(\vec{r},t\right) = \frac{\Gamma}{4\pi c}\frac{\partial}{\partial t}\left(\frac{1}{ct}\int_{S\left(\vec{r}',t\right)} H\left(\vec{r}'\right) dS'\left(t\right)\right); \left|\vec{r}-\vec{r}'\right| = ct, \tag{2}$$

where $S'(t)$ represents a spherical surface centered at a detector (located at $\vec{r}$) with radius vt as illustrated in Figure 1(a).

The pixel intensity in XACT images, reconstructed from captured X-ray-induced acoustic (XA) signals, reflects the X-ray energy deposition distribution. To get more accurate reconstruction compared with the traditional back projection, model-based XACT algorithm is used[34–37]

In discrete domain, the XA measurements $p^{(q)}$ at a q^{th} detector at all time steps can be expressed in the following way[34,36]:

$$\underline{p}^{(q)} = \boldsymbol{Q}^{(q)}\underline{h}, \tag{3}$$

where $\boldsymbol{Q}^{(q)}$ is a matrix dependent upon the distance of node in the 3D grid from the transducer, and vt as illustrated in Figure 1(a). The full XA measurement vector $\underline{p}$ (size: $N_d.\ N_t.1; N_d$: number of detectors, N_t : number of timesteps) can thus be expressed as:

$$\underline{p} = \mathbf{M}\underline{h}.,\ \mathbf{M} = \left[\boldsymbol{Q}^{(1)^T}, \boldsymbol{Q}^{(2)^T}, \ldots, \boldsymbol{Q}^{(N_d)^T}\right]^T \tag{4}$$

with $\mathbf{M}$ being the model-matrix with dimension: $(N_d.N_t) \times N$ where N is the number of voxels. In the inverse problem, we evaluate the X-ray energy deposition $\underline{h}$ from the measures XA signal from $\underline{p}_{meas}$ by solving the least squares problem:

$$\hat{\underline{h}} = \arg\min_{\underline{h}} \left|\left|\underline{p}_{meas} - \boldsymbol{M}\underline{h}\right|\right|_2^2 + \lambda^2 \left|\left|\boldsymbol{L}\underline{h}\right|\right|_2^2, \tag{5}$$

where $\boldsymbol{L}$ is the regularization matrix. The size of the model-matrix is typically too large, storing M requires a lot of memory. Therefore instead of directly computing M, we compute $\mathbf{M}\underline{u}$ and $\mathbf{M}^{\mathbf{T}}\underline{v}$ on-the-fly iteratively[36] Thus, the efficiency of iterative execution in calculating $\mathbf{M}\underline{u}$ and $\mathbf{M}^{\mathbf{T}}\underline{v}$ is directly affecting the reconstruction and imaging speed.

2.2 | GPU-accelerated 3D XACT image reconstruction

Implementing GPU-accelerated code is important to achieve high imaging speed, and potentially real-time imaging. Model-based XACT reconstruction algorithm is

24734209, 2026, 4, Downloaded from https://aapm.onlinelibrary.wiley.com/doi/10.1002/mp.70401 by University Of California Irvine Science Library Serials, Wiley Online Library on [30/10/2026]. See the Terms and Conditions (https://onlinelibrary.wiley.com/terms-and-conditions) on Wiley Online Library for rules of use; OA articles are governed by the applicable Creative Commons License

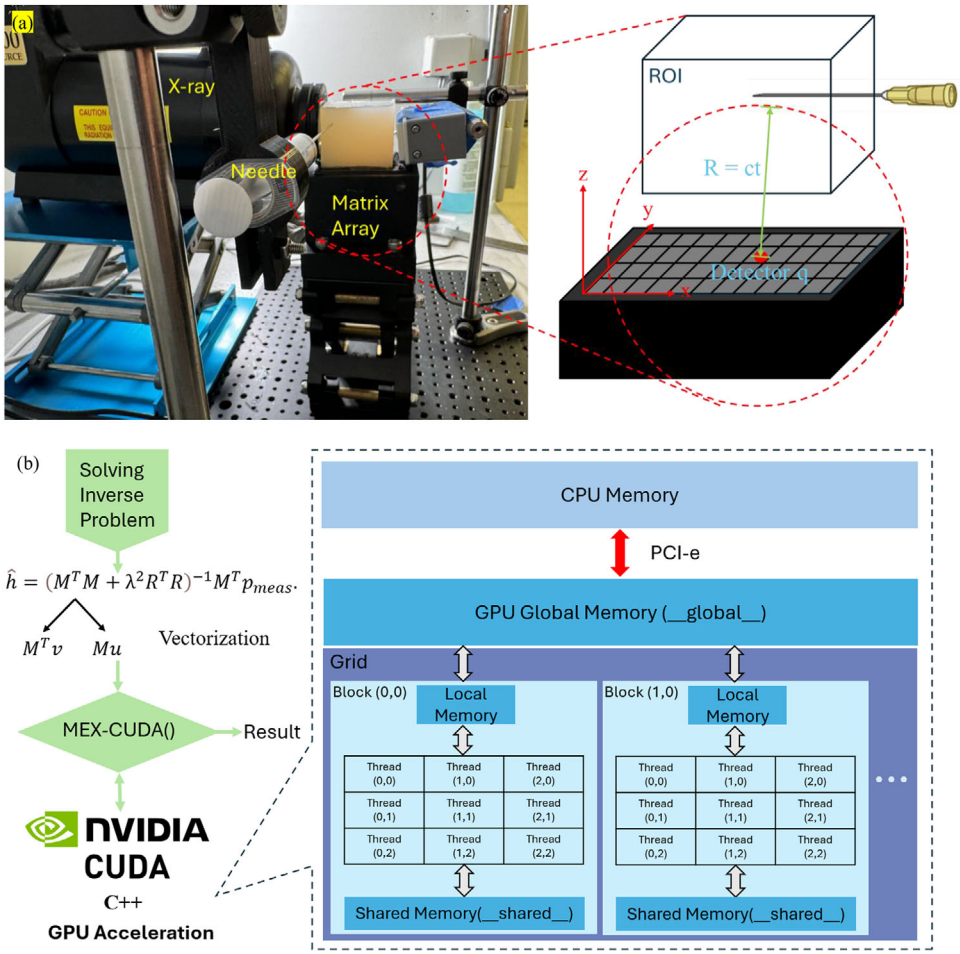

FIGURE 1 GPU-accelerated 3D XACT image reconstruction. (a) 3D XACT imaging system setup and reconstruction geometry, R denotes the distance from the detector q to the node in the 3D reconstruction grid of the region of interest (ROI); detector q is any elements of the 256 elements in the matrix/planar US array. (b) Pipeline flow of the CUDA-accelerated Model-based XACT algorithm. Variables defining the detection settings(such as reconstruction grid, detector coordinates, sampling frequency … etc.). In CUDA, the matrix waiting for calculation is first transferred from CPU memory to GPU global memory, then divided into each individual thread with corresponding to each individual cores in the GPU for parallel computation; After the calculation is done, it then transfers back to the GPU global memory and then back to CPU for further processing. Through the implementation of mexcuda libraries, C++ based GPU accelerated code can be used in Matlab.

based on the MATLAB platform[34,36] However, the built-in parallel computing tools provided by MATLAB were either insufficient in speed for our specific application or lacked fine-grained control over individual processing units, limiting opportunities for performance optimization. To address this, a MexCUDA-based implementation in C++ was integrated via the MATLAB[35,38,39]

The workflow of the GPU-accelerated model-based reconstruction is illustrated in Figure 1(b). Performance profiling revealed that the operations involving and $M^T v$ and Mu computation of the model matrix dominates the computational cost, with a time complexity of $O(n^2)$ which n is primarily dependent on the number of pixels and the sensor number. Consequently, optimization efforts were focused on accelerating this component.

The CUDA-based reconstruction pipeline in Figure 1(b) proceeds as follows:

1. The core C++ code is compiled into a .cu executable using the Mexcuda compiler and placed within the MATLAB working directory.
2. The vectorized variables(detector and pixel coordinates … etc.) are converted to gpu_Array() objects in MATLAB to facilitate transfer to the GPU memory space.
3. The mexcuda function accesses input variables from the MATLAB workspace by referencing pre-allocated pointers in the GPU memory.
4. Parallel computation is distributed across 256 threads per block, with the total block size determined by the number of iterations required for image reconstruction, which depends on the voxel count of the target image.
5. Atomic operations are employed within the CUDA kernels to prevent race conditions.

24734209, 2026, 4, Downloaded from https://aapm.onlinelibrary.wiley.com/doi/10.1002/mp.70401 by University Of California Irvine Science Library Serials, Wiley Online Library on [30/10/2026]. See the Terms and Conditions (https://onlinelibrary.wiley.com/terms-and-conditions) on Wiley Online Library for rules of use; OA articles are governed by the applicable Creative Commons License

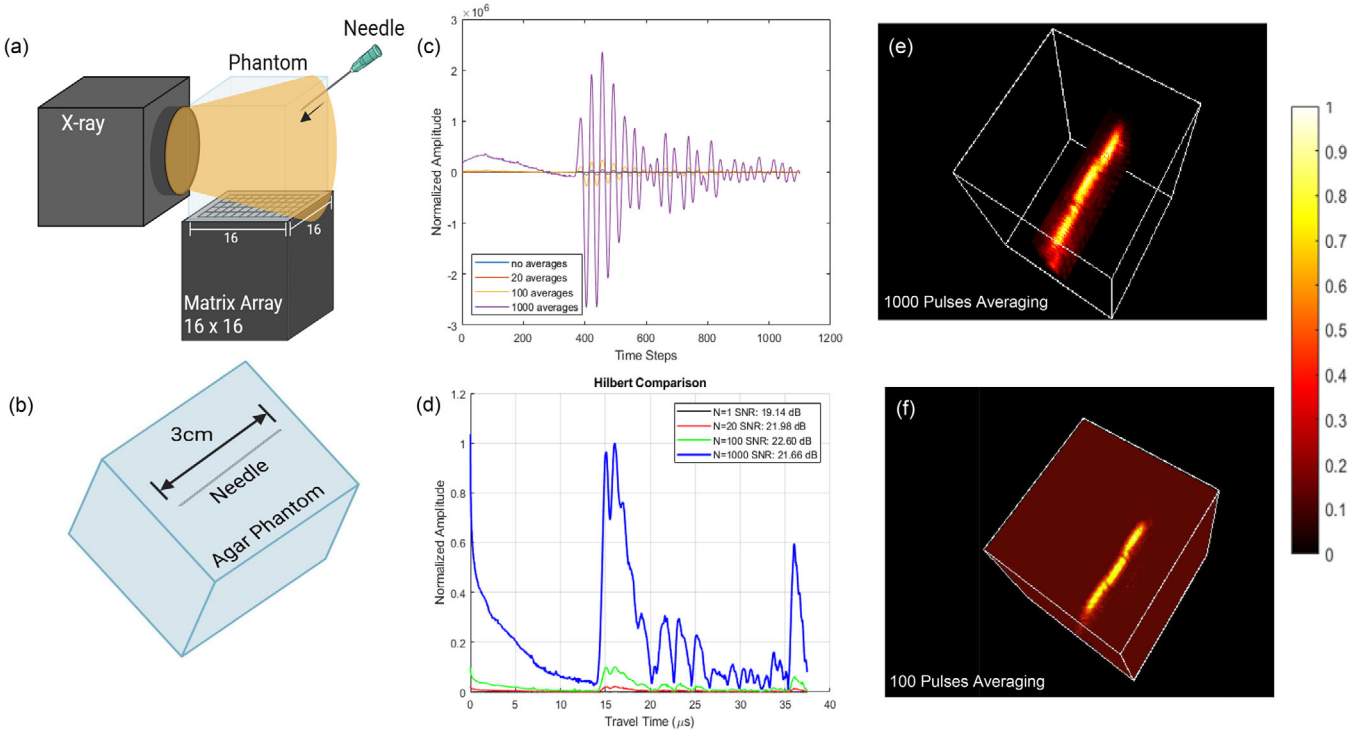

FIGURE 2 3D XACT imaging system in imaging the therapeutic needle. (a) the XACT experimental setup for 3D imaging, the 16 × 16 element US matrix array is placed 90 degrees to the X-ray beam (b) Shows the phantom setup, 14-gauge(2 mm) stainless-steel needle is embedded in a 3% agar phantom, the length is 3 cm. (c) Comparison of the detected XA signals with no average - 20 averages - 100 averages and 1000 averages, X-axis represents time steps sampled at 40 MHz sampling rate. (d) Hilbert-envelope of the coherently summed RF signal (Channel 121) for $N = 1,20,100$, and 1000pulses. SNR values are reported in the legend. (e) 3D reconstructed image from the needle with 1000 average. (f) 3D reconstructed image from 100 pulses.

6. Upon completion, the processed data are transferred from the GPU's shared memory back to the CPU.

All computations were performed on a workstation equipped with a 6-core AMD Ryzen 5 5600X CPU and an Nvidia Quadro P1000 GPU, featuring 640 CUDA cores and compute capability 6.1. The implementation was carried out using Microsoft Visual C++ 2019 and CUDA Toolkit version 11.7.0.

2.3 | XACT imaging systems

2.3.1 | 3D XACT imaging system

Figure 2(a) depicts the experimental setup for 3D XACT imaging system, comprising an X-ray excitation source and a 256 elements planar/matrix geometry US array system (Doppler Co. Limited, Guangzhou, China) with a center frequency of 1 MHz and a bandwidth of 60%. The captured signals were processed using a 256-channel data acquisition (DAQ) system (LEGION 256, PhotoSound Technologies Inc., Houston, USA). The X-ray source used is a pulsed generator (XR200, Golden Engineering, IN, USA), positioned to deliver horizontally directed X-ray pulses toward the imaging target. A tissue-mimicking agar phantom or pork belly sample is placed within the beam path and aligned above the US array.

For each experiment, a single or multiple 50 ns X-ray pulse is utilized to ensure precise energy deposition and mitigate cumulative radiation exposure. The system is capable of a 10 Hz repetition rate; however, the repetition rate is not strictly stable and exhibits occasional upward fluctuations.

Figure 2(c)–(e) illustrate the effects of background noise and pulse averaging on the signal-to-noise ratio (SNR) and image reconstruction. Figure 2(c) demonstrates the impact of XA signal averaging on the measured time-domain waveform. As the number of averaged frames N increases (1, 20, 100, and 1000), the baseline fluctuations are progressively suppressed and the XA waveform becomes more clearly discernible. This behavior is consistent with the expected benefit of ensemble averaging: for predominantly uncorrelated noise, the noise level decreases approximately as $1/\sqrt{N}$, yielding an SNR improvement that scales roughly with $\sqrt{N}$. The corresponding quantitative SNR values are summarized in Figure 2(d). At large N (e.g., 1000 averages), the SNR improvement becomes less pronounced, likely because residual correlated/non-random disturbances do not average

24734209, 2026, 4, Downloaded from https://aapm.onlinelibrary.wiley.com/doi/10.1002/mp.70401 by University Of California Irvine Science Library Serials, Wiley Online Library on [30/10/2026]. See the Terms and Conditions (https://onlinelibrary.wiley.com/terms-and-conditions) on Wiley Online Library for rules of use; OA articles are governed by the applicable Creative Commons License

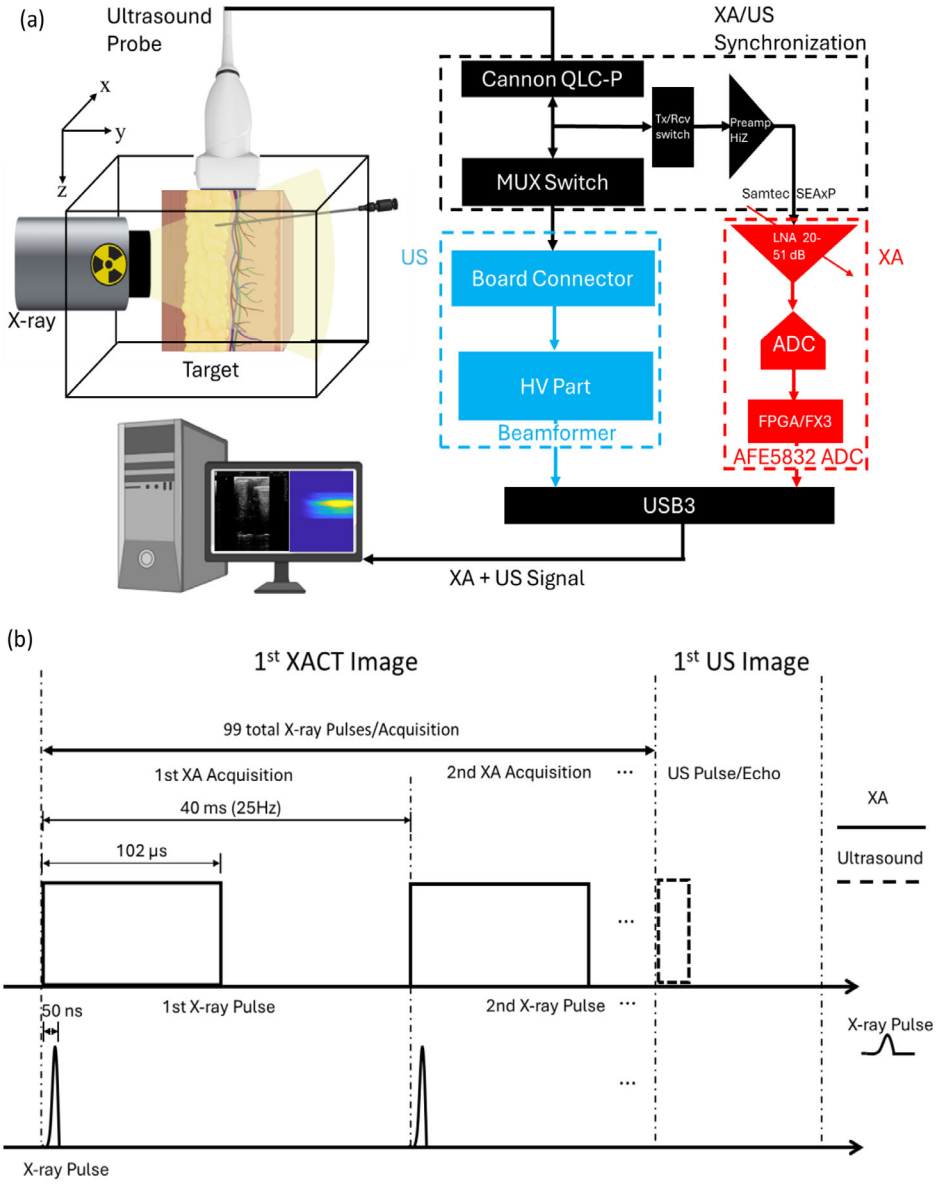

FIGURE 3 Dual-modality XACT/US system setup. (a) The schematic illustrates the internal configuration of the dual-modality acquisition system. The system integrates 128 channels capable of operating in both pulse-echo and receive-only modes, with built-in preamplifiers (AFE 5832 Texas Instruments, Dallas, TX, USA). A transmit/receive (Tx/Rcv) switch is incorporated to synchronize DAQ between XA and US modes, enabling auto switching the preamplifier between 2 different modes. (b) Timing diagram of the X-ray pulse, XA acquisition and US acquisition. X-ray pulse firing, XA acquisition and US acquisition are synchronized that after 100 XA signal acquisition, 1 US images is taken. The whole pipeline flow is controlled through a python control program.

out as effectively. Overall, reconstructions with $N \gtrsim 100$ pulse averages provide high-contrast, high-quality results (Figure 2(f) in comparison with 1000 pulses reconstruction (Figure 2(e)).

2.3.2 | Dual modal XACT and US imaging system

To enable dual-modality XACT/US imaging, a dual modality XA/US acquisition system (PhotoSound Technologies Inc., Houston, USA) was developed for both XA and US imaging (Figure 3(a)). Since XA signals are typically much weaker than the traditional pulse-echo US signals, a dedicated preamplifier of 51 dB gain is required to boost the XA signal to a detectable level[15,19] In contrast, conventional pulse-echo US imaging generally does not require such amplification due to the inherently stronger echo signals. To address these differing signal requirements without the need to manually swap the preamplifier between XA and US acquisitions, the DAQ system incorporates an integrated Tx/Rcv switch that toggles between transmit/receive and receive-only modes. This design not only ensures

24734209, 2026, 4, Downloaded from https://aapm.onlinelibrary.wiley.com/doi/10.1002/mp.70401 by University Of California Irvine Science Library Serials, Wiley Online Library on [30/10/2026]. See the Terms and Conditions (https://onlinelibrary.wiley.com/terms-and-conditions) on Wiley Online Library for rules of use; OA articles are governed by the applicable Creative Commons License

appropriate signal conditioning for each modality but also streamlines the workflow and reduces the time between XA and US acquisition down to almost zero which enables dual-modal imaging simultaneously. A clinically approved 128-element US probe(L12-5N40-A4, 5–12 MHz, Telemed, Milan, Italy) is incorporated into the system, and US images are captured using the clinically validated software EchoWave (Telemed Ultrasound, Milan, Italy). The dual-modal XA/US DAQ is synchronized as shown in Figure 3(b) with the X-ray pulse through a self-made scintillator circuit and a function generator (33600A, Keysight, Santa Rosa, USA). After 100 X-ray pulses with 100 XA signal acquisition, the Tx/Rcv switch is toggled, and changed to US mode where one US image is recorded. In the proposed dual-modality system, XACT and US data are acquired using the same probe with nearly simultaneous timing, resulting in inherent spatial co-registration. This intrinsic alignment enables direct fusion of XACT functional contrast with US anatomical information. A pork belly tissue was used to demonstrate XACT's potential future capabilities of in vivo imaging.

2.3.3 | Imaging protocols

To mimic human muscle properties, the experiments shown in Figures 1–3 utilized targets embedded within 3% agar phantoms (Difco™, Becton, Dickinson and Company, NJ, USA) as the imaging medium, providing both US coupling and human muscle-mimicking properties.

In this study, XACT measurements were performed using a pulsed portable X-ray source (Golden Engineering XR200) synchronized with the US acquisition system. According to the manufacturer specifications, the XR200 output is approximately 2.6–3 mR per pulse measured at 12 inches from the source. During each imaging sequence, the XR200 delivered discrete X-ray pulses at a repetition rate of 10 Hz, and the resulting X-ray–induced acoustic emissions were recorded by the US transducer for subsequent reconstruction. In all experiments, the X-ray source operated at a fixed projection angle, while the US probe was positioned at 90-degree angle or 180-degree relative to the X-ray beam direction. The acquisition window on the DAQ system was configured with varying samples per trigger pulse at a constant sampling frequency of 40 MHz. The system's maximum sampling provides a coverage of approximately 15.3 cm and a sound propagation duration roughly of 102 μs, ensuring sufficient temporal and spatial range to capture all generated signals. The filtering parameters for the X-ray–induced acoustic tomography (XACT) RF data differed slightly between the 2D and 3D systems. For denoising, the raw RF signals were first corrected for DC offset by subtracting the temporal mean of each channel. Channels exhibiting abnormal amplitude or saturated responses (indicative of atypical sensitivity) were excluded. The remaining data were then averaged across the acquired frames to improve SNR. Finally, the signals were band-pass filtered to suppress low-frequency disturbances (e.g., mechanical motion and power-line interference) and high-frequency electromagnetic interference (EMI). For the 256-element matrix array, a 0.5–1.5 MHz band-pass filter was applied. In contrast, for the 128-element linear array, a 5–12 MHz band-pass filter was applied to match the transducer bandwidth. All signal preprocessing and filtering were implemented in MATLAB.

3 | RESULTS

3.1 | 3D XACT imaging on monitoring of needle placement in human mimic phantom

An initial 3D needle monitoring experiment was conducted to evaluate the system's ability to track the insertion of a therapeutic needle as shown in Figure 4. The imaging volume was chosen as a 5 cm × 5 cm × 5 cm cube, providing sufficient spatial coverage to observe the full trajectory of the needle during insertion. To ensure precise and controlled advancement, the needle was mounted on a linear motor stage, which enabled fine adjustments of both insertion force and distance. The needle was advanced in incremental steps of 3 mm, ensuring accurate spatial tracking of the needle tip within the imaging volume.

For each imaging step, the reconstructed image was averaged over 100 X-ray pulses to enhance the SNR and improve overall image quality. To further refine image quality, background noise and back-reflection artifacts—particularly signals originating from regions far outside the true target location—were selectively removed from the acquired data. Additionally, a band-pass filter was applied during post-processing to suppress unwanted frequency components and enhance the detectability of the needle within the tissue-mimicking phantom. This comprehensive experimental setup provided high-fidelity, dynamic 3D images of the needle insertion process and established a strong foundation for future investigations focused on real-time interventional guidance.

3.2 | 3D XACT imaging of contrast agent dynamics

A 3D visualization experiment was performed to demonstrate the system's ability to image the dynamic flow of contrast agent (Omnipaque 300™, iohexol, GE HealthCare) within a blood vessel-mimicking phantom. The

24734209, 2026, 4, Downloaded from https://aapm.onlinelibrary.wiley.com/doi/10.1002/mp.70401 by University Of California Irvine Science Library Serials, Wiley Online Library on [30/10/2026]. See the Terms and Conditions (https://onlinelibrary.wiley.com/terms-and-conditions) on Wiley Online Library for rules of use; OA articles are governed by the applicable Creative Commons License

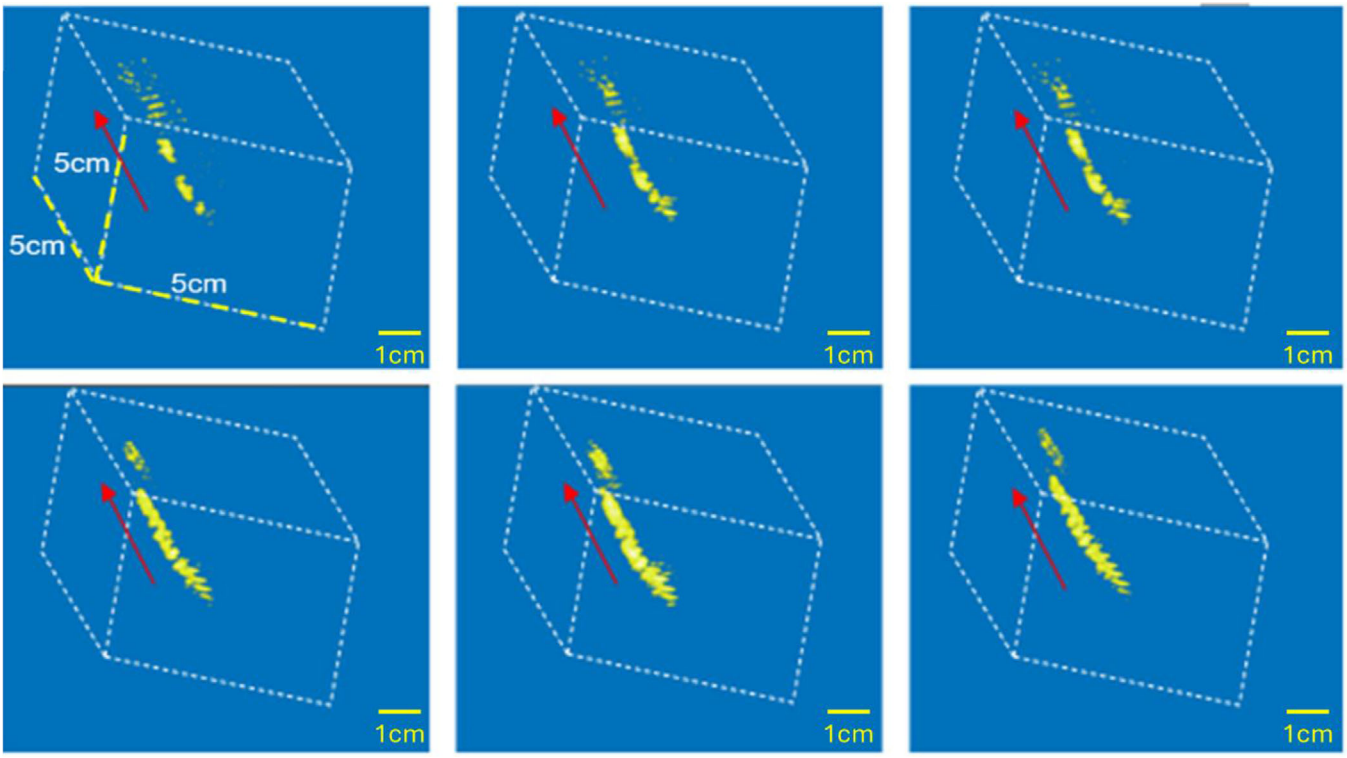

FIGURE 4 3D XACT therapeutic needle monitoring. The reconstructed imaging volume covered a 5 cm × 5 cm × 5 cm cube. The needle was advanced using a linear motor stage, allowing precise control over insertion force and distance to minimize the formation of large air channels caused by inconsistent needle movement. The insertion was performed in 3 mm increments, matching the lateral resolution limit of the transducer array.

contrast agent was injected into a silicone tube designed to simulate a blood vessel, with an inner diameter of 2.5 mm. To precisely control both the flow rate and the position of the contrast bolus within the imaging volume, the agent was advanced using a therapeutic needle connected to a pump system. This setup allowed for fine regulation of the flow speed and ensured accurate, reproducible positioning of the contrast agent within the tube (Figure 5(b)). An initial fully filled contrast agent static image is shown in Figure 5(c) to demonstrate the complete U-shaped tube in XACT. For dynamic XACT images, the injection was maintained at a constant rate of 10 mL per minute, providing a steady flow that enabled clear visualization of the contrast agent as it moved through the vessel-mimicking structure (Figure 5(a)). This experiment highlights the system's potential for high-resolution, dynamic 3D imaging of contrast flow, which is essential for applications in vascular imaging and interventional guidance.

3.3 | Dual modality XACT/US of the needle placement in soft tissue

The needle insertion was demonstrated on real tissue to validate the feasibility of XACT in the interventional procedure. To mimic human tissue properties, a pork belly sample was chosen for its similarities with human skin, fat, and muscle layers. A 14-gauge(2 mm) therapeutic needle was inserted through the skin into the tissue (Figure 6(a)). To prevent strong acoustic reflections caused by the water–air interface, the inside of the needle was filled with water, minimizing impedance mismatch effects. Precise needle insertion was controlled using a linear motor stage (DDS220, Thorlabs Inc., Newton, USA), advancing the needle in 3 mm increments. The L12-5L40N-A4 probe was positioned on the top of a pork belly with a thin layer of US gel to ensure proper acoustic coupling, while the X-ray beam was directed from the side, perpendicular to the insertion axis. After each needle advancement, 100 X-ray pulses were delivered and recorded by the DAQ system, followed by US image acquisition. The XACT image was reconstructed using an average of over 100 pulses per frame. A FWHM measurement performed on the LSF of the XACT image reveals that, with an average over 100 pulses, the system achieves a lateral resolution of approximately 2.3 mm (Figure 6(b)). The initial 4 frames of the dual-modality XACT/US are shown in Figure 6(c), Needle insertions at depths of 1 mm, 4 mm, 7 mm, and 10 mm into pork belly tissue were visualized using XACT. Concurrently, US imaging provided

24734209, 2026, 4, Downloaded from https://aapm.onlinelibrary.wiley.com/doi/10.1002/mp.70401 by University Of California Irvine Science Library Serials, Wiley Online Library on [30/10/2026]. See the Terms and Conditions (https://onlinelibrary.wiley.com/terms-and-conditions) on Wiley Online Library for rules of use; OA articles are governed by the applicable Creative Commons License

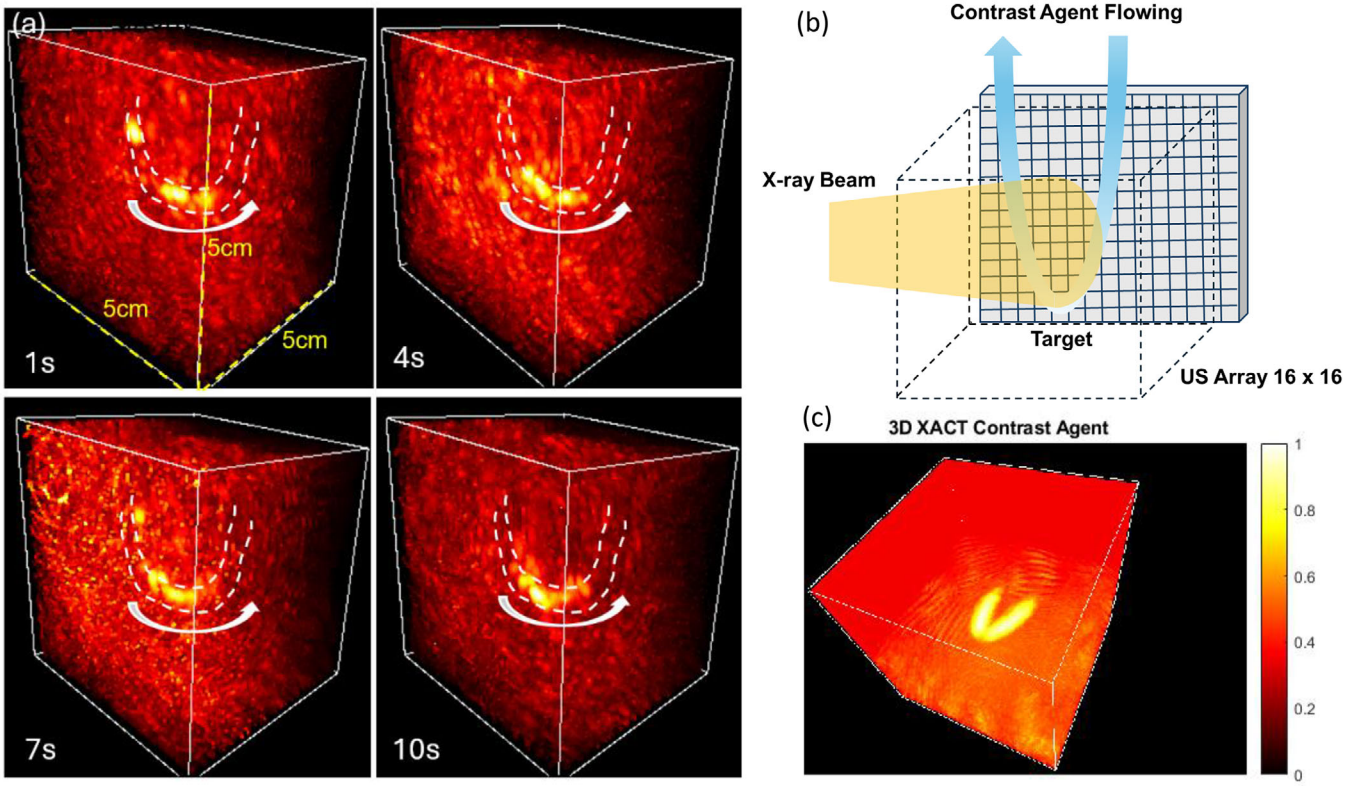

FIGURE 5 3D XACT of the X-ray contrast agent monitoring (a) Contrast agent (Omnipaque 300™ iohexol, GE HealthCare). is injected into a silicone blood-vessel mimicking tube and pushed with a therapeutic needle controlled by a pump to precisely control the flow-speed therefore the location of the tube. The inner diameter of the tube is 2.5 mm, and the contrast agent is injected at the constant rate of the 10 mL per minute. (b) System set up of the 3D dynamic contrast agent experiment, the contrast agent is circulating with water mixing towards a fixed direction at a constant flow rate within the U-shaped tube. The X-ray beam is hitting perpendicularly to the U-shape tube, and the matrix US detector is placed after the U-shaped tube. (c) A static 3D XACT image of the U-shaped tube when it's filled with X-ray contrast agent completely with 100 pulses averages.

complementary background information of the surrounding tissue. Currently, the overlay of XACT and US soft tissue background is performed manually using MATLAB; however, future work aims to incorporate advanced automated deep-learning-based image registration techniques.

4 | DISCUSSION

In summary, our study demonstrated the feasibility of using XACT as a fast, 3D imaging modality for IR applications, including needle guidance and contrast agent monitoring. The results validate that XACT, when integrated with US to form a dual-modality system, can provide complementary information by utilizing the strengths of both acoustic and radiological imaging approaches. Compared to traditional cone-beam CT, XACT offers several unique advantages. First, XACT enables true 3D imaging without the need for rotational scanning[20] thereby eliminating motion artifacts and reducing procedural delays inherent in CBCT workflows[40] Moreover, the use of short-pulse X-ray excitation allows for rapid DAQ with less dosage, achieving imaging speeds up to 1 frame per 3–4 s—limited currently by the pulse repetition rate of the X-ray source and the acoustic SNR. This feature opens the possibility of near real-time imaging in dynamic interventional procedures, a capability not currently achievable with CBCT or traditional fluoroscopy.[41] Furthermore, the integration of XACT with conventional US provides an innovative imaging platform that enhances soft tissue visualization while simultaneously offering high-contrast tracking of radio-opaque objects such as needles and contrast agents. This dual-modality approach may address long-standing challenges in US-guided interventions, where acoustic artifacts, limited viewing angles, and poor needle conspicuity often compromise procedural safety and efficacy.

Nonetheless, several limitations should be acknowledged. The current system provides ~2 mm effective resolution, which is sufficient for proof-of-concept contrast localization and coarse needle guidance and is on the same order as the few-millimeter targeting

24734209, 2026, 4, Downloaded from https://aapm.onlinelibrary.wiley.com/doi/10.1002/mp.70401 by University Of California Irvine Science Library Serials, Wiley Online Library on [30/10/2026]. See the Terms and Conditions (https://onlinelibrary.wiley.com/terms-and-conditions) on Wiley Online Library for rules of use; OA articles are governed by the applicable Creative Commons License

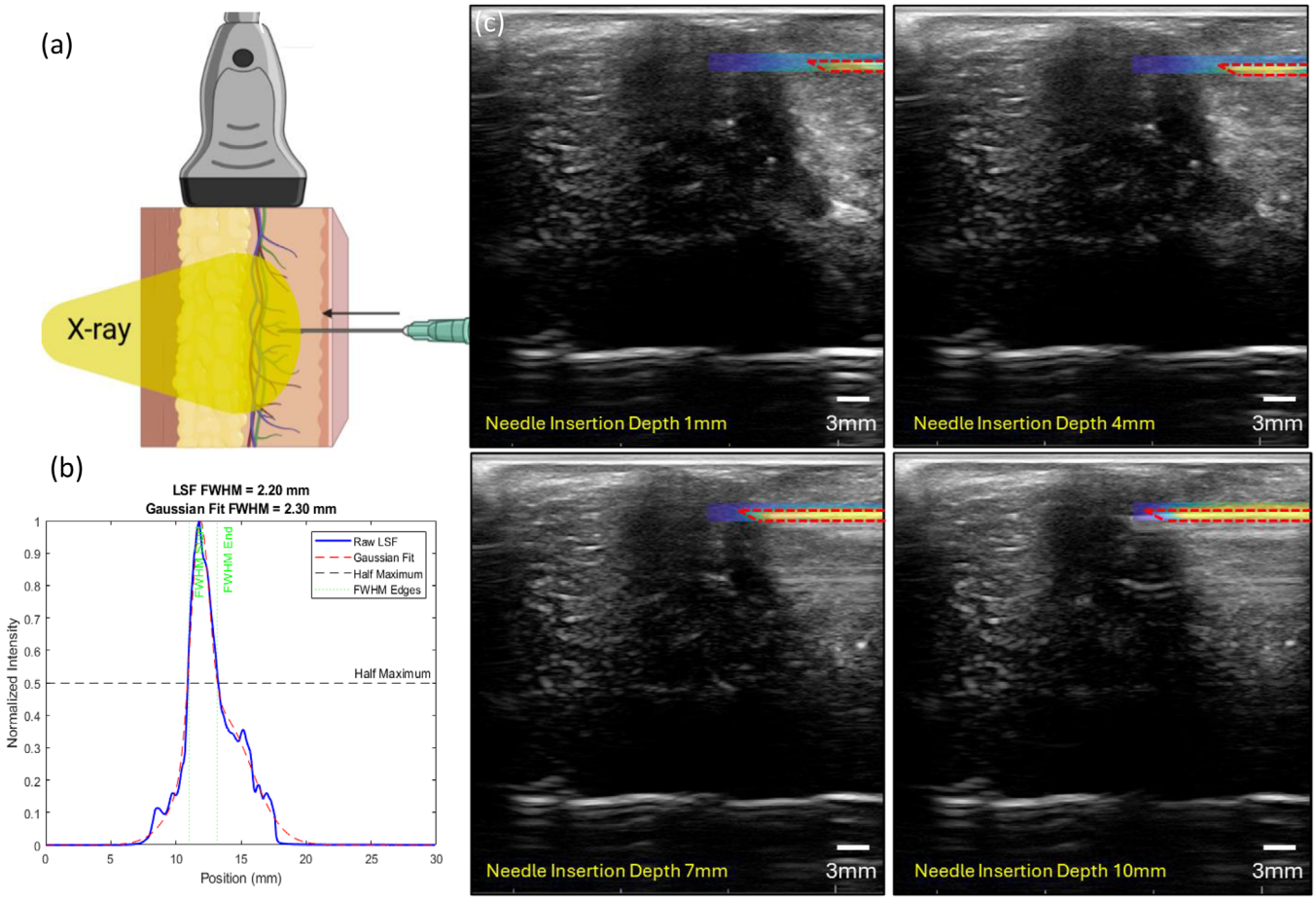

FIGURE 6 Dual-modality imaging with XACT. (a) Schematic of the experimental setup. (b) Plotting of the Line Spread Function (LSF). Full-Width Half Maximum (FWHM) of the XACT's line profile and the gaussian fit line, the resolution is around 2–3 mm. (c) Representative video frame of the 2D US image overlaid with the XACT image. The US image captured using commercial software (EchoWave II, Telemed ultrasound, Milan, Italy) with the L12-5L40N-A4 array, provides anatomical details of tissue layers (fat, muscle), while XACT enhances needle contrast dynamically (100 averages, ~4 s per frame).

accuracy commonly required in many needle-based interventions. Future work will improve image fidelity via bandwidth/aperture optimization and limited-view mitigation to support more demanding tasks (e.g., small-lesion and margin-sensitive targeting).The current imaging speed, although significantly faster than conventional CT, is still constrained by the X-ray system's repetition rate and the need for signal averaging to achieve clinically acceptable image quality. Moreover, while the spatial resolution XACT achieved is sufficient for gross anatomical guidance, further optimization is required to improve the resolution toward sub-millimeter levels, required for fine-needle interventions. Another critical aspect yet to be addressed is that the current system relies on a portable pulsed X-ray generator (XR200), which, while convenient and compact, inherently suffers from a low repetition rate (up to 10 Hz) and a relatively small focal spot size. The low repetition rate limits the achievable imaging speed, making real-time continuous imaging challenging, especially for rapidly changing events such as needle adjustments. Finally, the small hotspot of the X-ray restricts the field of view and requires multiple re-positionings to cover larger anatomical regions[42] The absence of an active cooling mechanism in the X-ray source further imposes thermal constraints on prolonged imaging sessions. After short imaging sessions, the X-ray tube requires an enforced cooling period of approximately 3–4 min to prevent thermal damage, severely restricting workflow efficiency and precluding continuous or prolonged imaging sequences. This limitation not only impacts the practicality of XACT in dynamic procedures but also introduces workflow interruptions that may be incompatible with clinical interventional timelines. The current experimental validation was conducted using simplified tissue phantoms, which do not fully replicate the X-ray attenuation or acoustic properties of biological tissue. As such, the presented results primarily demonstrate system feasibility under controlled conditions. In addition, dual-modality imaging is currently demonstrated in a two-dimensional

24734209, 2026, 4, Downloaded from https://aapm.onlinelibrary.wiley.com/doi/10.1002/mp.70401 by University Of California Irvine Science Library Serials, Wiley Online Library on [30/10/2026]. See the Terms and Conditions (https://onlinelibrary.wiley.com/terms-and-conditions) on Wiley Online Library for rules of use; OA articles are governed by the applicable Creative Commons License

configuration. Ongoing work focuses on extending the framework to fully three-dimensional imaging and evaluating performance with advanced DAQ system in more realistic models to establish clinical relevance. Furthermore, while the proposed framework is compatible with 2D matrix arrays for volumetric dual-modality imaging, practical implementation introduces additional challenges, including increased data-transfer bandwidth, channel multiplexing, and careful timing-sequence design. In particular, XACT requires low-noise preamplifiers whereas conventional US does not, necessitating a robust switching scheme to prevent high-voltage transmit pulses from damaging the receive circuitry.

These hardware constraints underscore the need for future system improvements, such as the development of high-repetition-rate, actively cooled X-ray sources with larger and uniform beam profiles suitable for volumetric imaging over extended durations. In the future, emerging X-ray technologies, such as those based on Laser Wakefield Acceleration (LWFA), hold the potential to address these limitations by providing ultrashort pulse widths, significantly higher repetition rates[43] and narrower energy spectra[44,45] Such sources could enable true real-time 3D XACT imaging with improved temporal resolution, and enhanced image quality due to their quasi-monochromatic nature.

Furthermore, the needle insertion procedure could be automated using a more precise robotic arm[46–48] reducing reliance on manual operation. Conventional US-guided needle tracking heavily depends on the physician's expertise and hand-eye coordination, which can introduce variability in accuracy and procedure success rates[49] This reliance becomes even more challenging under radiological conditions, where physicians are exposed to ionizing radiation, further limiting procedure time and increasing occupational risks. Acoustic window limitations may also affect dual-modality XACT–US imaging, since XACT detection relies on an unobstructed acoustic path between the emission region and the receive aperture. In clinically relevant anatomies, probe placement constraints and highly reflective/attenuating structures (e.g., bone) can reduce angular coverage and SNR, leading to limited-view artifacts. Future work will investigate optimized probe positioning and integrated probe geometries to maximize acoustic access and mitigate these effects. Integrating a robotic-assisted system with real-time imaging guidance—such as XACT—has the potential to enhance procedural precision, reduce operator dependency, and improve safety by enabling remote or shielded operation away from the radiation field.

Additionally, the manual overlay of XACT and US images, although feasible in the current study, poses a workflow bottleneck and may introduce misregistration errors. Future studies should focus on developing automated, real-time fusion pipelines, potentially using artificial intelligence-based registration and visualization frameworks.

5 | CONCLUSION

This study represents the first demonstration of dynamic, 3D XACT and Dual Modality imaging for IR applications, including needle placement guidance and dynamic contrast agent monitoring. The dual-modality approach combining XACT and US offers a promising imaging platform that leverages the strengths of both modalities to enhance procedural safety and accuracy.

However, some limitations persist, notably the constraints imposed by the current X-ray source's low repetition rate, small focal spot, and lack of active cooling, which results in mandatory cooling periods to prevent tube damage. These issues represent critical barriers to the clinical translation of XACT and underscore the need for system-level optimizations. Future work will prioritize the development of high-performance, actively cooled X-ray systems, improvements in imaging speed and spatial resolution, and the integration of advanced real-time dual-modality visualization tools. In vivo studies are also essential to establish the clinical feasibility and utility of XACT in guiding complex interventional procedures where existing modalities remain inadequate.

In conclusion, both the dual-modality and 3D XACT demonstrate significant potential for reliable application in clinical IR, offering enhanced procedural accuracy and serving as a valuable complement to existing imaging technologies.

ACKNOWLEDGMENTS

This work was supported by the National Institutes of Health (R37CA240806, U01CA288351, R50CA283816). The authors would like to acknowledge the support from UCI Chao Family Comprehensive Cancer Center (No. P30CA062203). The content is solely the responsibility of the authors and does not necessarily represent the official views of the National Institutes of Health. Approximately, $500k of federal funds supported the effort (50%) on this project.

CONFLICT OF INTEREST STATEMENT

Dr. Liangzhong Xiang has financial interest in SoundDose, Inc., which, however, did not support this work. Dr Abi-Jaoudeh has declared conflict of interests with the following entities: she is the principal investigator on research grants and/or clinical trials at University of California that are sponsored or have received financial support from Innova Vascular Inc, Medtronic Inc, Penumbra Inc, Teclison Limited Inc, Guerbet SA, Varian Inc, ABK Biomedical, Impact Biotech Inc., Innova Vascular Inc., Instylla HES Inc, Sirtex Medical Ltd. Dr Abi-Jaoudeh has served on advisory boards, speaker bureau or consulted with Genentech F. Hoffmann-La Roche Ltd, AstraZeneca Inc., Eisai Inc., ABK Biomedical Inc., Instylla HES Inc., SIRTEX Inc., Boston Scientific, Inc,

24734209, 2026, 4, Downloaded from https://aapm.onlinelibrary.wiley.com/doi/10.1002/mp.70401 by University Of California Irvine Science Library Serials, Wiley Online Library on [30/10/2026]. See the Terms and Conditions (https://onlinelibrary.wiley.com/terms-and-conditions) on Wiley Online Library for rules of use; OA articles are governed by the applicable Creative Commons License

Guerbet SA., Replimune Inc., Terumo Inc., RenovoRx Inc., IVQIA Inc., Angiodynamics Inc., Varian Inc. These activities are unrelated to the subject matter of this work.

DATA AVAILABILITY STATEMENT

The data that support the findings of this study are available from the corresponding author upon reasonable request.

REFERENCES

1. De Jong TL, Van De Berg N, Tas L, Moelker A, Dankelman J, Van Den Dobbelsteen J. Needle placement errors: do we need steerable needles in interventional radiology?. *MDER*. 2018;11:259–265. doi:10.2147/MDER.S160444
2. Morgan R, Cleveland T, Hamady M, et al. Interventional radiology in the 21st century: planning for the future. *Clin Radiol*. 2021;76(12):865–869. doi:10.1016/j.crad.2021.10.001
3. Dhanik A, Stenson BA, Levenson RB, Antkowiak PS, Sanchez LD, Chiu DT. Root cause analysis of delayed emergency department computed tomography scans. *West J Emerg Med*. 2024;25(2):226–229. doi:10.5811/westjem.17831
4. Naksuk N, Padmanabhan D, Asirvatham SJ. Cardiac anatomy for catheter mapping and ablation of arrhythmias. In: Huang SKS, Miller JM, eds. *Catheter Ablation of Cardiac Arrhythmias*. Elsevier; 2019:54–74.e4. doi:10.1016/B978-0-323-52992-1.00005-3
5. Ng P, McGowan M, Goldstein M, Kassardjian CD, Steinhart BD. The impact of CT head scans on ED management and length of stay in bizarre behavior patients. *Am J Emerg Med*. 2018;36(2):213–217. doi:10.1016/j.ajem.2017.07.080
6. Van Lent WAM, Deetman JW, Teertstra HJ, Muller SH, Hans EW, Van Harten WH. Reducing the throughput time of the diagnostic track involving CT scanning with computer simulation. *Eur J Radiol*. 2012;81(11):3131–3140. doi:10.1016/j.ejrad.2012.03.012
7. Kilcoyne RF, Richardson ML, Porter BA, Olson DO, Greenlee TK, Lanzer W. Magnetic resonance imaging of soft tissue masses. *Clin Orthop Relat Res*. 1988(228):13–19. doi:10.1097/00003086-198803000-00002
8. Hollingsworth KG. Reducing acquisition time in clinical MRI by data undersampling and compressed sensing reconstruction. *Phys Med Biol*. 2015;60(21):R297–R322. doi:10.1088/0031-9155/60/21/R297
9. Horga G, Kaur T, Peterson BS. Annual research review: current limitations and future directions in MRI studies of child- and adult-onset developmental psychopathologies. *J Child Psychol Psychiatry*. 2014;55(6):659–680. doi:10.1111/jcpp.12185
10. Yan Z, Li L, Qiu R, Chen Z. Research on X-ray fluorescence enhanced fluoroscopy imaging technology. *Photonics*. 2021;8(10):441. doi:10.3390/photonics8100441
11. Nardi C, Molteni R, Lorini C, et al. Motion artefacts in cone beam CT: an *in vitro* study about the effects on the images. *BJR*. 2016;89(1058):20150687. doi:10.1259/bjr.20150687
12. Kalabalık F, Aytuğar E, Aykanat F, Çiftçi C. Repetition rate of scanning due to motion artefacts in cone-beam computed tomography: a retrospective study. *J Oral Maxillofac Res*. 2024;15(1):e6. doi:10.5037/jomr.2024.15106
13. Nayak KS, Lim Y, Campbell-Washburn AE, Steeden J. Real-time magnetic resonance imaging. *J Magn Reson Imaging*. 2022;55(1):81–99. doi:10.1002/jmri.27411
14. Racadio JM, Babic D, Homan R, et al. Live 3D Guidance in the interventional radiology Suite. *Am J Roentgenol*. 2007;189(6):W357–W364. doi:10.2214/AJR.07.2469
15. Yan Y, Xiang S(Liangzhong. X-ray-induced acoustic computed tomography and its applications in biomedicine. *J Biomed Opt*. 2023;29(S1). doi:10.1117/1.JBO.29.S1.S11510
16. Samant P, Trevisi L, Ji X, Xiang L. X-ray induced acoustic computed tomography. *Photoacoustics*. 2020;19:100177. doi:10.1016/j.pacs.2020.100177
17. Xiang L, Tang S, Ahmad M, Xing L. High resolution X-ray-induced acoustic tomography. *Sci Rep*. 2016;6(1):26118. doi:10.1038/srep26118
18. Xiang L, Han B, Carpenter C, Pratx G, Kuang Y, Xing L. X-ray acoustic computed tomography with pulsed x-ray beam from a medical linear accelerator. *Med Phys*. 2013;40(1):010701. doi:10.1118/1.4771935
19. Wang S, Ivanov V, Pandey PK, Xiang L. X-ray-induced acoustic computed tomography (XACT) imaging with single-shot nanosecond x-ray. *Appl Phys Lett*. 2021;119(18):183702. doi:10.1063/5.0071911
20. Wang S, Pandey PK, Lee G, et al. X-ray–induced acoustic computed tomography: 3D X-ray absorption imaging from a single view. *Sci Adv*. 2024;10(49):eads1584. doi:10.1126/sciadv.ads1584
21. Tang S, Yang K, Chen Y, Xiang L. X-ray-induced acoustic computed tomography for 3D breast imaging: a simulation study. *Med Phys*. 2018;45(4):1662–1672. doi:10.1002/mp.12829
22. Zheng Y, Samant P, Merill J, et al. X-ray-induced acoustic computed tomography for guiding prone stereotactic partial breast irradiation: a simulation study. *Med Phys*. 2020;47(9):4386–4395. doi:10.1002/mp.14245
23. Li Y, Samant P, Cochran C, et al. The feasibility study of XACT imaging for characterizing osteoporosis. *Med Phys*. 2022;49(12):7694–7702. doi:10.1002/mp.15906
24. Li Y, Samant P, Wang S, Behrooz A, Li D, Xiang L. 3-D X-Ray-induced acoustic computed tomography with a spherical array: a simulation study on bone imaging. *IEEE Trans Ultrason, Ferroelect, Freq Contr*. 2020;67(8):1613–1619. doi:10.1109/TUFFC.2020.2983732
25. Robertson E, Samant P, Wang S, Tran T, Ji X, Xiang L. X-Ray-induced acoustic computed tomography (XACT): initial experiment on bone sample. *IEEE Trans Ultrason, Ferroelect, Freq Contr*. 2021;68(4):1073–1080. doi:10.1109/TUFFC.2020.3032779
26. Sun L, Gonzalez G, Pandey PK, et al. Towards quantitative in vivo dosimetry using x-ray acoustic computed tomography. *Med Phys*. 2023;50(11):6894–6907. doi:10.1002/mp.16476
27. Choi S, Park EY, Park S, Kim JH, Kim C. Synchrotron X-ray induced acoustic imaging. *Sci Rep*. 2021;11(1):4047. doi:10.1038/s41598-021-83604-3
28. Choi S, Park S, Pyo A, et al. In situ x-ra y-induced acoustic computed tomography with a contrast agent: a proof of concept. *Opt Lett*. 2022;47(1):90. doi:10.1364/OL.447618
29. Chen H, Rogalski MM, Anker JN. Advances in functional X-ray imaging techniques and contrast agents. *Phys Chem Chem Phys*. 2012;14(39):13469–13486. doi:10.1039/c2cp41858d
30. Heck L, Herzen J. Recent advances in X-ray imaging of breast tissue: from two- to three-dimensional imaging. *Physica Medica*. 2020;79:69–79. doi:10.1016/j.ejmp.2020.10.025
31. Zhou Y, Yao J, Wang LV. Tutorial on photoacoustic tomography. *J Biomed Opt*. 2016;21(6):061007. doi:10.1117/1.JBO.21.6.061007
32. Wang LV. Tutorial on photoacoustic microscopy and computed tomography. *IEEE J Select Topics Quantum Electron*. 2008;14(1):171–179. doi:10.1109/JSTQE.2007.913398
33. Xu M, Wang LV. Photoacoustic imaging in biomedicine. *Review of Scientific Instruments*. 2006;77(4):041101. doi:10.1063/1.2195024
34. Pandey PK, Wang S, Aggrawal HO, Bjegovic K, Boucher S, Xiang L. Model-based X-Ray-induced acoustic computed tomography. *IEEE Trans Ultrason, Ferroelect, Freq Contr*. 2021;68(12):3560–3569. doi:10.1109/TUFFC.2021.3098501
35. Ding L, Razansky D, XL Dean-Ben. Model-based reconstruction of large three-dimensional optoacoustic datasets. *IEEE*

24734209, 2026, 4, Downloaded from https://aapm.onlinelibrary.wiley.com/doi/10.1002/mp.70401 by University Of California Irvine Science Library Serials, Wiley Online Library on [30/10/2026]. See the Terms and Conditions (https://onlinelibrary.wiley.com/terms-and-conditions) on Wiley Online Library for rules of use; OA articles are governed by the applicable Creative Commons License

Trans Med Imaging. 2020;39(9):2931–2940. doi:10.1109/TMI.2020.2981835
36. Pandey PK, Wang S, Sun L, Xing L, Xiang L. Model-based 3-D X-Ray induced acoustic computerized tomography. *IEEE Trans Radiat Plasma Med Sci*. 2023;7(5):532–543. doi:10.1109/TRPMS.2023.3238017
37. Dean-Ben XL, Buehler A, Ntziachristos V, Razansky D. Accurate model-based reconstruction algorithm for three-dimensional optoacoustic tomography. *IEEE Trans Med Imaging*. 2012;31(10):1922–1928. doi:10.1109/TMI.2012.2208471
38. Dean-Ben XL, Ozbek A, Razansky D. Volumetric real-time tracking of peripheral human vasculature with GPU-accelerated three-dimensional optoacoustic tomography. *IEEE Trans Med Imaging*. 2013;32(11):2050–2055. doi:10.1109/TMI.2013.2272079
39. Lee D, Park EY, Choi S, et al. GPU-accelerated 3D volumetric X-ray-induced acoustic computed tomography. *Biomed Opt Express*. 2020;11(2):752. doi:10.1364/boe.381963
40. Floridi C, Radaelli A, Abi-Jaoudeh N, et al. C-arm cone-beam computed tomography in interventional oncology: technical aspects and clinical applications. *Radiol Med*. 2014;119(7):521–532. doi:10.1007/s11547-014-0429-5
41. Krompaß K, Mutschler M, Grunz JP, et al. Real-time dosimetry in interventional radiology—comparing the occupational radiation exposure in fluoroscopy-guided lower extremity and abdominal procedures. *Eur Radiol*. April 13 2025;35:6575–6582. doi:10.1007/s00330-025-11566-5. Published online.
42. Pétusseau A, Bruza P, Pogue BW. Nanosecond scanned x-ray sheet imaging for time-resolved luminescence tomography. In: Pogue BW, ed. *Optics and Ionizing Radiation*. SPIE; 2020:12. doi:10.1117/12.2544438
43. Song P, Barbrel B, Dorchies F, Courjaud A. A compact robust laser driven X-ray source for phase contrast imaging. In: *Optica high-brightness sources and light-driven interactions congress 2022*. Optica Publishing Group; 2022:ETh5A.4. doi:10.1364/EUVXRAY.2022.ETh5A.4
44. Fletcher LB, Zastrau U, Galtier E, et al. High resolution x-ray Thomson scattering measurements from cryogenic hydrogen jets using the linac coherent light source. *Rev Sci Instrum*. 2016;87(11):11E524. doi:10.1063/1.4959792
45. Aniculaesei C, Ha T, Yoffe S, et al. The acceleration of a high-charge electron bunch to 10 GeV in a 10-cm nanoparticle-assisted wakefield accelerator. *Matter Radiat. Extremes*. 2024;9(1):014001. doi:10.1063/5.0161687
46. Sutedjo V, Tirindelli M, Eilers C, Simson W, Busam B, Navab N. Acoustic shadowing aware robotic ultrasound: lighting up the dark. *IEEE Robot Autom Lett*. 2022;7(2):1808–1815. doi:10.1109/LRA.2022.3141451
47. Su K, Liu J, Ren X, et al. A fully autonomous robotic ultrasound system for thyroid scanning. *Nat Commun*. 2024;15(1):4004. doi:10.1038/s41467-024-48421-y
48. Spenkelink IM, Heidkamp J, Avital Y, Fütterer JJ. Evaluation of the performance of robot assisted CT-guided percutaneous needle insertion: comparison with freehand insertion in a phantom. *Eur J Radiol*. 2023;162:110753. doi:10.1016/j.ejrad.2023.110753
49. Di Serafino M, Iacobellis F, Schillirò ML, et al. Common and uncommon errors in emergency ultrasound. *Diagnostics*. 2022;12(3):631. doi:10.3390/diagnostics12030631

How to cite this article: Yan Y, Pandey PK, Xu Y, et al. XACT-guided interventional procedures: A feasibility study. *Med Phys*. 2026;53:e70401. https://doi.org/10.1002/mp.70401

24734209, 2026, 4, Downloaded from https://aapm.onlinelibrary.wiley.com/doi/10.1002/mp.70401 by University Of California Irvine Science Library Serials, Wiley Online Library on [30/10/2026]. See the Terms and Conditions (https://onlinelibrary.wiley.com/terms-and-conditions) on Wiley Online Library for rules of use; OA articles are governed by the applicable Creative Commons License